IEEE Robotics and Automation Letters (RA-L) paper, presented at ICRA 2026, Vienna, Austria. Cite as RA-L paper.

Fabrication and Characterization of Additively Manufactured Stretchable Strain Sensors Towards the Shape Sensing of Continuum Robots

Daniel C. Moyer[1], Wenpeng Wang[2], Logan S. Karschner[1], Loris Fichera[2], and Pratap M. Rao[1]

***Abstract*—This letter describes the manufacturing and experimental characterization of novel stretchable strain sensors for continuum robots. The overarching goal of this research is to provide a new solution for the shape sensing of these devices. The sensors are fabricated via direct ink writing, an extrusion-based additive manufacturing technique. Electrically conductive material (i.e., the *ink*) is printed into traces whose electrical resistance varies in response to mechanical deformation. The principle of operation of stretchable strain sensors is analogous to that of conventional strain gauges, but with a significantly larger operational window thanks to their ability to withstand larger strain. Among the different conductive materials considered for this study, we opted to fabricate the sensors with a high-viscosity eutectic Gallium-Indium ink, which in initial testing exhibited high linearity ($R^2 \approx 0.99$), gauge factor ≈ 1, and negligible drift. Benefits of the proposed sensors include (*i*) ease of fabrication, as they can be conveniently printed in a matter of minutes; (*ii*) ease of installation, as they can simply be glued to the outside body of a robot; and (*iii*) ease of miniaturization, which enables integration into millimeter-sized continuum robots.**

***Index Terms*—Soft Sensors and Actuators, Surgical Robotics: Steerable Catheters/Needles**

I. Introduction

CONTINUUM Robots are a class of flexible, slender manipulators that can bend and twist continuously along their length, allowing them to navigate through complex and tortuous spaces. Research interest in these robots has increased tremendously over the last fifteen years, as documented in a recent survey by Russo *et al.* [1]. Continuum robots hold considerable potential in numerous applications, including interventional medicine [2], [3], industrial inspection and repair [4], [5], and underground exploration [6].

Shape sensing is crucial for the control and navigation of continuum robots. By monitoring their shape, continuum robots can perform tasks with high accuracy, avoid obstacles, and have safe interactions with humans. A comprehensive survey (up to 2016) of shape sensing methods for continuum robots can be found in the review by Shi and colleagues [7]. Existing approaches include, among others, methods based on computer vision [8]–[13], electromagnetic tracking [14]–[16], and Fiber-Bragg Grating [17]–[20]. It is also possible to implement shape sensing by integrating traditional strain gauges (i.e., strain gauges that consist of a metal foil bonded onto a flexible plastic sheet) into the body of a continuum robot, e.g., [21]. This solution is appealing because strain gauges are relatively inexpensive and straightforward to use. However, the body of a continuum robot can experience large deformations that exceed the operational strain limits of traditional strain gauges (typically less than 1% [22]). Therefore, measures need to be taken to prevent the sensors from breaking, such as installing them into semi-rigid enclosures (as in [21]), which adds to the complexity of their integration and use. Furthermore, it can be a challenge to install strain gauges in the body of some continuum robots, particularly those developed for surgical applications, due to their minuscule size.

To overcome these challenges, in this letter, we propose to explore the use of resistive *stretchable strain sensors*. This is

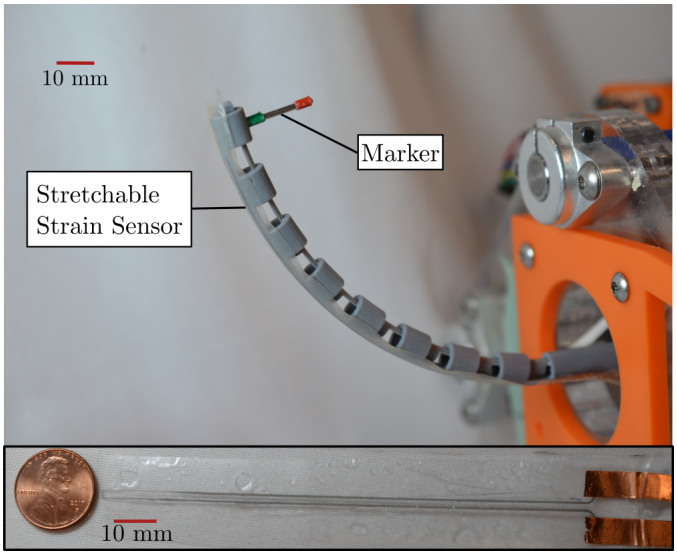

Fig. 1. (Top): Stretchable strain sensor installed onto a concentric push-pull robot [23]. (Bottom): Sensor specimen. The strain sensors we describe in this letter can withstand much larger strains than traditional strain gauges and are therefore suitable for installation on the exterior surface of a continuum robot.

Manuscript received: December 19, 2024; Revised March 20, 2025; Accepted April 30, 2025.

This paper was recommended for publication by Editor Cecilia Laschi upon evaluation of the Associate Editor and Reviewers' comments. This material is based upon work partially supported by the National Science Foundation under Grant numbers 1922761 and 2341532. Any opinions, findings, and conclusions or recommendations expressed in this material are those of the author(s) and do not necessarily reflect the views of the National Science Foundation. The first two authors contributed equally to this work. *(Corresponding author: Wenpeng Wang)*

[1]D.C. Moyer, L.S. Karschner and P.M. Rao are with the Department of Mechanical and Materials Engineering, Worcester Polytechnic Institute, Worcester, MA 01609, USA.

[2]W. Wang and L. Fichera are with the Department of Robotics Engineering, Worcester Polytechnic Institute, Worcester, MA 01609, USA. wwang11@wpi.edu

Digital Object Identifier (DOI): see top of this page.

IEEE Robotics and Automation Letters (RA-L) paper, presented at ICRA 2026, Vienna, Austria. Cite as RA-L paper.

a class of sensing devices that consist of a thin and highly stretchable electrically conductive material [24], [25]. The principle of operation is analogous to that of a conventional strain gauge (i.e., deformations of the sensor produce a change in electrical resistance), but with a larger operational window. Within robotics, these sensors are currently being explored for applications in soft prosthetics and wearable devices, as well as the monitoring of soft robotic grippers and actuators [26]–[28]. In this letter, we show that these sensors are also suitable for estimating the bending of continuum manipulators (see Fig. 1), thus providing a new option for the shape sensing of these devices.

Throughout the remainder of this letter, we describe the design, fabrication, and experimental characterization of novel stretchable strain sensors for continuum robots. The sensors are manufactured via direct ink writing, a rapid prototyping method in which the conductive material (i.e., the *ink*) is additively printed into a prescribed shape, similar to the process used in extrusion-based 3D printers [25]. We first report the results of a study aimed at identifying a suitable conductive ink out of a set of three candidate materials, namely a silver-elastomer composite, a carbon-elastomer composite, and a gallium-indium-based liquid metal composite. We then introduce stretchable strain sensors for two types of continuum manipulators, i.e., a push-pull concentric tube robot [29] (⌀ 8 mm), and a notched-tube continuum wrist [30] (⌀ 1.1 mm).

II. Sensor Fabrication and Evaluation of the Conductive Inks

Figure 2 shows three stretchable strain sensors printed for this study, each using a different conductive ink. The suitability of each ink for the application at hand was investigated via cyclic loading experiments in which the sensors were repeatedly stretched as if they were attached to the body of a continuum robot. The sensors were evaluated in terms of linearity, drift, and gauge factor.

A. Sensor Fabrication

The sensors were fabricated via direct ink writing using the V-One printer (Voltera Inc., Waterloo, ON, Canada), equipped with a $0.23\,\mathrm{mm}$ diameter nozzle. Print settings used in this work were: pass spacing of $0.15\,\mathrm{mm}$, dispensing height of $0.08\,\mathrm{mm}$, feed rate of $500\,\mathrm{mm/min}$, and trim length of $25\,\mathrm{mm}$. This nozzle and these print settings result in a trace width of $0.3\,\mathrm{mm}$ per pass. Each sensor was printed onto a thermoplastic polyurethane (TPU) film (ESTANE® FS H92C4P, Lubrizol Corporation, Wickliffe, OH, USA), which serves as the base layer. This specific TPU film was chosen because of its large maximum recoverable strain (quoted to be 350%), its good adhesion to the three conductive inks chosen for this study (which is introduced in the next section), and its higher rigidity compared to other grades of TPU, which facilitates the handling of the sensors after printing. The sensor specimens used in this study were printed in batches of 4, with a total manufacturing time of approximately 30 minutes per batch, including the necessary post-processing time for each ink type specified below.

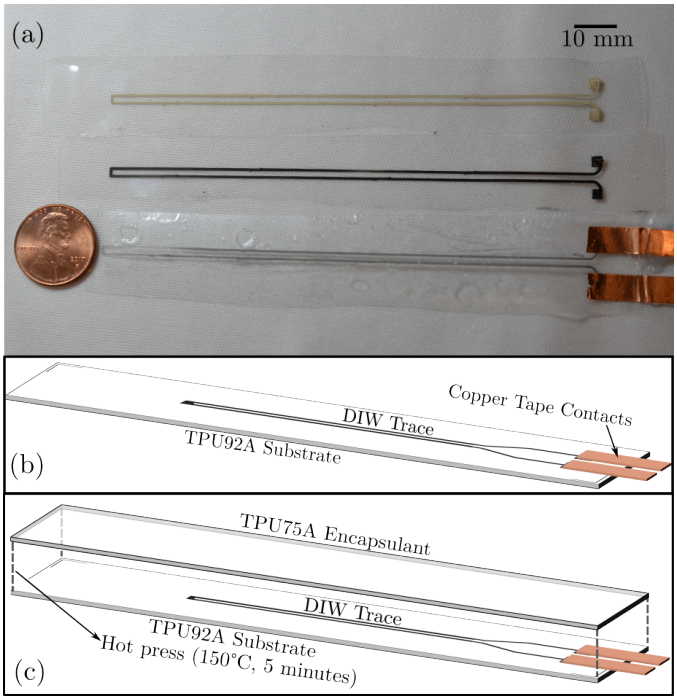

Fig. 2. (a) Stretchable strain sensors manufactured with different conductive materials: (Top) Silver-based sensor; (Middle) Carbon-based sensor; (Bottom) Gallium-Indium (ELMNT®) sensor. Sensor dimensions are $112\,\mathrm{mm}$ (length), $2.2\,\mathrm{mm}$ (width), with a trace width of $0.6\,\mathrm{mm}$. For further specifications on these materials, refer to Table I. (b) Schematic showing the structure of conductor-elastomer composite based sensors. (c) Schematic for liquid metal based sensors.

TABLE I
Conductive Ink Types used for the Fabrication of the Stretchable Strain Sensors

Name	Ink Type	Conductive Material
SE 1109	Conductor-elastomer composite	Silver
SE 1502	Conductor-elastomer composite	Carbon
ELMNT® ST	Liquid metal	Gallium-indium eutectic

After completing the necessary post-processing, the sensors were attached to the desired surface using hot melt TPU film (ESTANE® FS HM70A71, Lubrizol Corporation, Wickliffe, OH, USA) as an adhesive layer between the sensor substrate and the desired surface. The bonding was then completed by pressing the assembly in a $1050\,\mathrm{W}$ hot press (TLM38385, Vevor, Rancho Cucamonga, CA, USA) at $130\,^{\circ}\mathrm{C}$ for 30 seconds to melt the TPU and ensure a robust bond.

B. Conductive Ink Types

Table I lists the three conductive inks evaluated in this study and used in the fabrication of the sensors shown in Fig. 2. These inks were selected from a pool of materials known to be well-suited for the fabrication of stretchable electronics [31]. We narrowed down the pool by requiring that materials be commercially available, suitable for printing on TPU substrates, and rated for maximum elongation of, at least, 100%. Finally, we required materials to be compatible with direct ink writing on the V-One printer.

IEEE Robotics and Automation Letters (RA-L) paper, presented at ICRA 2026, Vienna, Austria. Cite as RA-L paper.

While all the inks listed in Table I are off-the-shelf and commercially available, we note that none of them is specifically marketed for creating strain sensors—instead, they are intended for printing conductive or resistive traces in electronic circuits; therefore, the inks are being evaluated here for a different application than the one they were originally intended for.

1) Conductor-elastomer Composite Inks: The SE 1109 and the SE 1502 (ACI Materials, Goleta, CA, USA) are elastomeric inks with conductive particles embedded into them — silver and carbon, respectively. Sensors using these inks are cured, post-printing, by placing them in an oven heated at $140\,^{\circ}\mathrm{C}$ for 5 minutes.

The operation of stretchable strain sensors based on conductor-elastomer inks is explained by the *electrical percolation* phenomenon [32], [33], i.e., when the material is stretched, the conductive particles embedded therein are pulled apart from each other, producing an increase in electrical resistance.

2) Liquid Metal Inks: The ELMNT® ST (UES Inc., Dayton, OH, USA) is a high-viscosity conductive ink based on a gallium-indium eutectic (eGaIn) alloy. Since eGaIn is liquid at room temperature, fabricating liquid metal sensors requires an additional step, as illustrated in Fig. 2(c): A second TPU film (ESTANE® FS L75A4P, Lubrizol Corporation, Wickliffe, OH, USA) is hot pressed ($150\,^{\circ}\mathrm{C}$, 5 minutes) on top of the printed sensor to form an airtight seal with the sensor's bottom TPU layer, encapsulating the liquid metal and preventing its escape. Furthermore, liquid metal sensors require a mechanical activation step, which involves either peeling off the TPU backing sheet or stretching the sensor to break the oxide shells on the liquid metal particles. Incomplete or imperfect activation can result in a higher electrical resistance during the initial cycles of operation.

For stretchable strain sensors utilizing liquid metal inks, the increase in resistance is attributed to the increase in length and decrease in the cross-sectional area of the conductive pathway.

C. Experimental Evaluation of the Conductive Inks

The sensors were evaluated as illustrated in Fig. 3: Each sensor was first attached with hot melt TPU to a flat, $3\,\mathrm{mm}$-thick beam made of Acrylonitrile Styrene Acrylate (ASA), which was then cyclically bent from straight to maximum deformation and then back to straight 50 times by means of a motorized stage. Three sensor specimens were prepared for each of the three inks, and their response was studied under four different experimental conditions, detailed in Table II and labeled (a-d), aimed to simulate different loading conditions that the sensors could experience in practical use. Experimental parameters include the strain at full bending, the strain rate, and the dwell time. Briefly, the strain at full bending describes the maximum deformation experienced by the sensor in each experiment. This parameter was controlled by regulating the displacement of the motorized stage, and thus the beam's curvature. As can be observed from Fig. 3(d), the strain distribution experienced by the beams during testing was predictable but not uniform, therefore Table II reports both peak and average values; the average value will be used in the characterization of the gauge factor, as explained below. The strain rate is defined as the ratio of the average strain to the time duration of each cycle. It quantifies the speed at which deformation occurs. This parameter was controlled by regulating the speed of the motorized stage that was bending the test beams (refer to Fig. 3). Finally, dwell time refers to the waiting period between two consecutive bending cycles.

TABLE II
EXPERIMENTAL CONDITIONS USED IN THE EVALUATION OF THE CONDUCTIVE INKS

ID	Strain Rate (s^{-1})	Dwell Time (s)	Peak Strain (%)	Average Strain (%)
(a)	0.027	1	2.91	1.36
(b)	0.054	5	2.91	1.36
(c)	0.026	5	9.66	2.63
(d)	0.052	1	9.66	2.63

The sensors were evaluated in terms of three performance metrics, namely gauge factor, drift, and linearity of the response.

1) Gauge Factor: The gauge factor (GF) is defined as

$$\mathrm{GF} = \frac{\Delta R/R_0}{\epsilon}. \tag{1}$$

where R_0 is the baseline electrical resistance of the sensor (i.e., the resistance under zero strain), ϵ is the applied strain, and ΔR is the observed change in resistance. For the purpose of this study, we estimate the GF by inputting the resistance change observed at full bending, and the average strain created along the body of the sensor, as listed in Table II. In general, a large GF is desirable, as it corresponds to a more responsive sensor.

2) Drift: Drift is a measure of how much the sensor's baseline electrical resistance R_0 changes over time. In stretchable strain sensors, drift is often linked to the progressive accumulation of plastic deformation in the sensor's material, which occurs as a result of repeated loading cycles at high strain levels. For the purpose of this study, we estimate drift as

$$\mathrm{Drift} = \frac{\Delta R_0/R_0}{\mathrm{cycle}}. \tag{2}$$

We wish to identify an ink that exhibits as little drift as possible, and exhibits a response to strain that significantly exceeds any drift that occurs within the operational window.

3) Linearity: Linearity is simply estimated by finding the line that best approximates the sensor's response and calculating the corresponding coefficient of determination (R^2). High linearity is generally desirable as it enables the simplest possible sensor calibration.

D. Results

The results of the ink evaluation experiments are summarized in Table III, which reports the average values observed for each experimental condition. The conductor-elastomer composite inks (silver and carbon) generally exhibited larger but highly variable GF values. The silver-based sensors

IEEE Robotics and Automation Letters (RA-L) paper, presented at ICRA 2026, Vienna, Austria. Cite as RA-L paper.

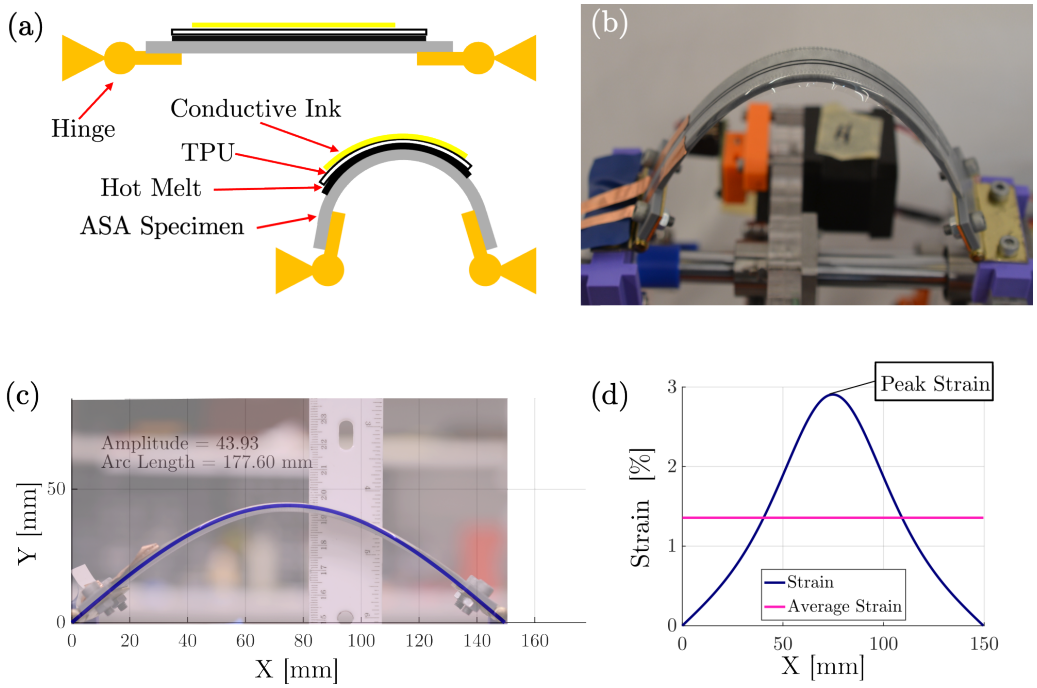

Fig. 3. Experimental apparatus and test for the evaluation of the conductive inks. (a) Schematic of the test setup. Each sensor is attached to an Acrylonitrile Styrene Acrylate (ASA) beam, which is controllably bent to simulate different loading conditions. (b) Actual ASA specimen under load with a sensor attached. Bending is achieved by attaching one of the two ends of the beam to a linear stage controlled by a stepper motor. The electrical resistance of the sensor is monitored with an IM3536 LCR meter (Hioki E.E. Corporation, Nagano, Japan), not pictured here. The position of the moving terminal of the linear stage was recorded using a magnetic linear encoder, the AS5048A-HTSP (ams OSRAM AG, Premstätten, Austria), and used to estimate the applied strain, as explained in the following. Both strain and resistance measurements were captured at 10 Hz and timestamped with Robot Operating System 2 (ROS 2) running on Ubuntu 20.04, on a laptop equipped with an i7-8750H CPU (Intel Corp., Santa Clara, CA, USA). (c) Beam shape reconstruction based on the applied load, using a simple model of beam buckling under compressive loads [34]. (d) Estimated strain distribution along the beam.

TABLE III
GAUGE FACTOR, DRIFT, AND LINEARITY OF THE PROPOSED SENSORS

Ink	Experimental Condition	GF	Drift ($\frac{\Delta R_0/R_0}{\text{cycle}}$)	Cycles†	Linearity (R^2)
SE 1109 (Silver)	(a)	3.0	9.7×10^{-4}	43	0.98
	(b)	3.5	1.3×10^{-3}	37	0.98
	(c)	15	2.1×10^{-2}	19	0.93
	(d)	14	1.2×10^{-2}	30	0.90
SE 1502 (Carbon)	(a)	5.5	-3.4×10^{-4}	2.2×10^{2}	0.93
	(b)	5.2	-4.5×10^{-4}	1.6×10^{2}	0.95
	(c)	2.0	1.9×10^{-4}	3.3×10^{3}	0.60
	(d)	1.8	-2.0×10^{-5}	2.4×10^{3}	0.60
ELMNT® ST	(a)	1.2	1.0×10^{-5}	1.6×10^{3}	0.98
	(b)	1.3	2.0×10^{-5}	9.0×10^{2}	0.99
	(c)	0.88	1.1×10^{-4}	2.1×10^{2}	0.99
	(d)	0.91	1.0×10^{-5}	2.4×10^{3}	0.99

†: Number of cycles after which the effect of drift becomes larger than the resistance change at full bending.

showed approximately a 5-fold change, while the carbon-based sensors exhibited about a 2.5-fold change over the tested ranges. Both sensors were significantly affected by drift. The plots in Fig. 4 show the sensors' responses under experimental condition (a) and visually illustrate the effect of drift on the sensor output. In practical use, these sensors would need frequent recalibration to compensate for drift, potentially as often as every 19 bending cycles for the silver-based sensor (see Table III). Interestingly, the carbon-based sensors exhibited significantly less drift when subjected to high strain (experimental conditions (c) and (d)), but also significant degradation in linearity under these conditions, with the R^2 score dropping to ≈ 0.6.

In contrast, the liquid metal sensors exhibited GFs ranging between 0.88 and 1.3 and demonstrated significantly better stability, with at most $\sim 1.5\times$ variation over the same tested ranges. Furthermore, these sensors exhibited high linearity across all experimental conditions ($R^2 > 0.98$) and significantly less drift than the conductor-elastomer sensors.

IEEE Robotics and Automation Letters (RA-L) paper, presented at ICRA 2026, Vienna, Austria. Cite as RA-L paper.

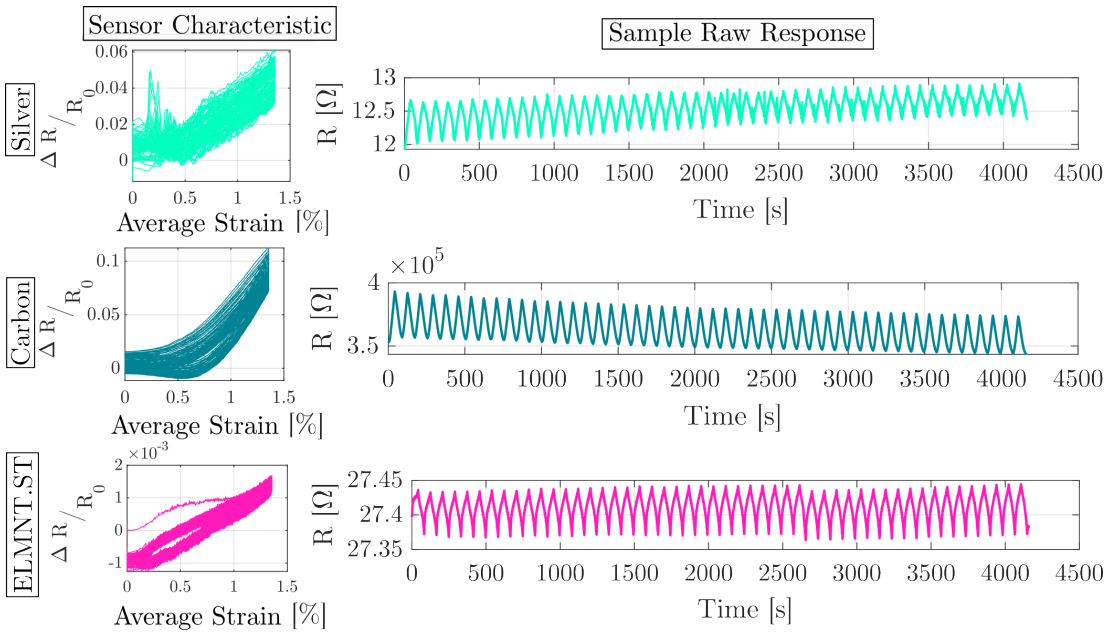

Fig. 4. Raw sensor output and characteristic curves observed under experimental condition (a). The sensor using the ELMNT® ink exhibited higher linearity and significantly less drift than the ones based on the conductor-elastomer composite inks (silver and carbon). The initial resistance of the ELMNT® sensor is slightly higher during the first cycle, attributed to imperfect mechanical activation.

E. Discussion

Numerous studies have investigated materials for fabricating stretchable strain sensors, as summarized in a recent survey by Zhao *et al.* [22]. Many of these studies focus on experimental nanomaterials that are typically available only at a laboratory scale. In contrast, in this work, we exclusively consider commercially available inks.

Carbon and silver elastomeric inks are composed of networks of conductive fillers embedded within an elastomeric matrix. While these networks can produce relatively high gauge factors (GF) when stretched, they are prone to damage and permanent deformation resulting in drift in electrical resistance. The elastomeric sensors discussed in this paper exhibit behavior similar to those described in the literature. For instance, Zhang and colleagues [35] studied stretchable strain sensors made of carbon and silver particles within a TPU matrix. These sensors achieved a GF ranging from 5 to 10 for strains up to 10% and exhibited drift in the order of 1 $\times$ 10^{-4} per cycle under repeated stretching at the same strain level. The GF of these sensors is comparable to that of the silver and carbon sensors tested in this study, while the drift results align with those observed for the carbon sensor but are smaller than those seen in the silver sensor.

In contrast to carbon and silver inks, ELMNT® ink is liquid at room temperature. The only significant drift affecting sensor performance stems from the TPU material on which the ELMNT® ink is printed and encapsulated, leading to minimized drift and more stable sensor behavior. The liquid metal sensors examined in this study can be compared to those described by Abbara and colleagues [27], who used a syringe-dispensing process to print ELMNT® liquid metal traces onto TPU substrates. The sensors in [27] use larger trace width (1 mm, compared to 0.6 mm in this study) and were tested under constant strain cycling while varying temperatures. These sensors demonstrated a GF of 1.2 to 1.4 (average 1.3) and exhibited negligible drift at room temperature. Similarly, the liquid metal sensors reported here achieved GFs of 1.2 to 1.3 under low peak strain conditions (2.91% peak strain in experimental conditions (a) and (b)), consistent with findings in [27]. However, under higher peak strain conditions (9.66% peak strain in experimental conditions (c) and (d)), the GF was slightly lower, at approximately 0.9. The variation in GF across strain ranges may be attributed to differences in TPU substrates or other, as yet unidentified, factors warranting further investigation. Notably, the sensors studied here maintained extremely low drift, consistent with the findings of [27].

Although the ELMNT® liquid metal sensors exhibited the lowest GF among the tested sensors, they proved to be the most suitable for shape sensing applications due to their negligible drift, which enables a clear and consistent sensor response. Additionally, their relatively uniform GF across varying experimental conditions, along with high sensor linearity, are important benefits. In the next section, we describe experimental work aimed to validate the viability of using liquid metal sensors for the shape sensing of continuum robots.

III. Shape Sensing Experiments

To study the suitability of liquid metal stretchable strain sensors for shape sensing, we performed experiments with two types of continuum robots, namely a concentric push-pull robot (CPPR) [23] and a notched tube wrist (NWT) [30]. These robots are shown in Fig. 1 and Fig. 5, respectively. Details on the actuation and the modeling of these devices are beyond the scope of this manuscript, and interested readers are referred to the papers cited above.

IEEE Robotics and Automation Letters (RA-L) paper, presented at ICRA 2026, Vienna, Austria. Cite as RA-L paper.

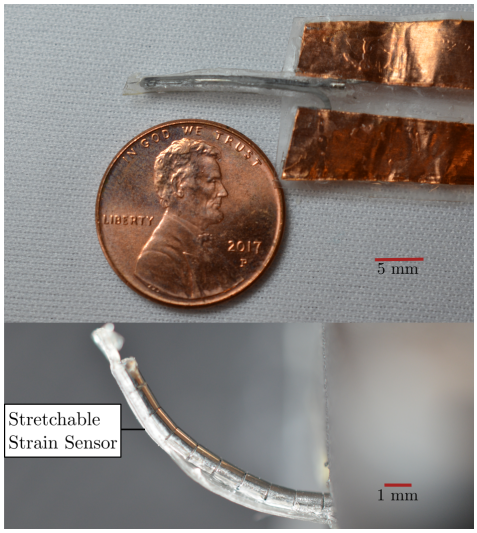

Fig. 5. (Top): ELMNT® stretchable strain sensors installed onto a notched tube wrist [30]. The sensing area measures 17 mm in length and 0.6 mm in width, with a trace width of 0.3 mm.

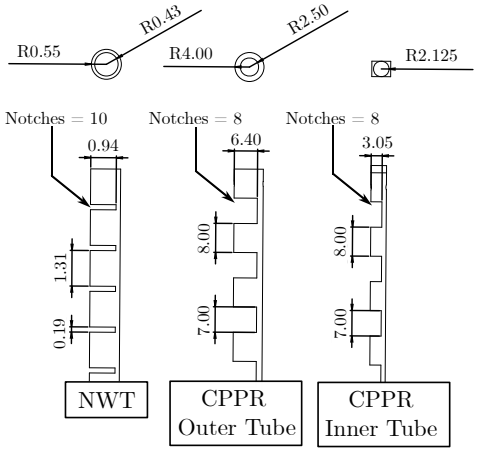

Fig. 6. Dimensions of the continuum robots utilized in this study. In this figure, R denotes radius of the tube. All dimensions are in millimeters, except for the notch count.

The body of the CPPR is made of ASA, and it was printed with a Bambu Lab X1 printer (Bambu Lab, Shenzen, PRC). The outer diameter of this robot is 8 mm. The NWT was manufactured by laser-cutting notches in the body of a thin Nickel-Titanium tube of diameter 1.1 mm. Laser cutting was outsourced to Resonetics LLC (San Diego, CA, USA). Other robot dimensions are listed in Fig. 6.

A. Procedure

The two manipulators were outfitted with a liquid metal stretchable strain sensor, which was attached to the outer surface with hot melt TPU as illustrated in Fig. 1 and Fig. 5, and were subsequently subjected to a cyclic loading experiment wherein they were bent up to their tightest bending radius. Each experiment was repeated three times, during which the sensor response was logged together with the manipulator bending angle. The bending angle of the robots was measured via image processing, using video footage captured with a RealSense D405 camera (Intel Corp., Santa Clara, CA, USA) at a resolution of 640 × 480 pixels. Both manipulators were outfitted with colored markers (visible in Fig. 1) in order to facilitate the detection of their tips during bending.

B. Results

Results are shown in Fig. 7 and Fig. 8 for the CPPR and the NWT, respectively. In these figures, sub-figure (a) displays resistive response to bending angle, (b) presents raw response of the sensor, and (c) illustrates the single-cycle relationship between the sensor output and the manipulator's bending angle.

IV. Discussion

Experimental findings suggest the viability of liquid metal stretchable strain sensors for the shape sensing of continuum robots. Experimental results reported in Figs. 7 and 8 show generally good linearity and repeatability, with some caveats as discussed in the following. It is important to note that the strain encountered by the sensors in these experiments was larger than the average strain encountered in earlier testing. In the continuum manipulators used for this study, the maximum strain is experienced on the outer surface of the robot's body. Using the relations from [36], we estimate the CPPR to have experienced a maximum strain of 3.15% at full bending, while the NWT experienced a maximum strain of 7.40%. These findings indicate that the sensors can effectively handle the strains experienced by continuum robots.

The data in Figs. 7 and 8 also reveal some undesirable effects. First, in sub-figures (a), there is noticeable hysteresis in the sensor response, particularly in the case of the experiment with the NWT. These results highlight the need for hysteresis compensation in order to achieve accurate sensor calibration. In a related study [37], a stretchable strain sensor—fabricated by mixing carbon black particles into liquid polyurethane rubber, followed by curing and cutting into strips—was employed for sensing and closed-loop control of a continuum robot. Although that sensor exhibited significant viscoelasticity, hysteresis, and creep, its behavior was effectively modeled. In future work, we plan to adopt a similar approach by implementing mathematical compensation models, such as the Preisach model [38], to characterize and compensate the hysteresis exhibited by our sensors.

Sensor response on the CPPR exhibited drift during the initial bending cycles, as can be observed in Fig. 7(b). We attribute such drift to an incomplete activation of the liquid metal ink prior to the experiment. As it was discussed earlier in the manuscript, each sensor needs to be *broken in* before use by means of repeated stretching. The purpose of this process is to fully break the insulating gallium oxide shell around the gallium indium liquid metal particles in the ink, allowing the liquid metal to form a continuous conductor. In cases of imperfect activation, some liquid metal particles retain their oxide shell. Then, during the first few cycles of operation, some of these remaining oxide shells break, resulting in the release of the liquid metal, which in turn leads to a decrease in resistance.

IEEE Robotics and Automation Letters (RA-L) paper, presented at ICRA 2026, Vienna, Austria. Cite as RA-L paper.

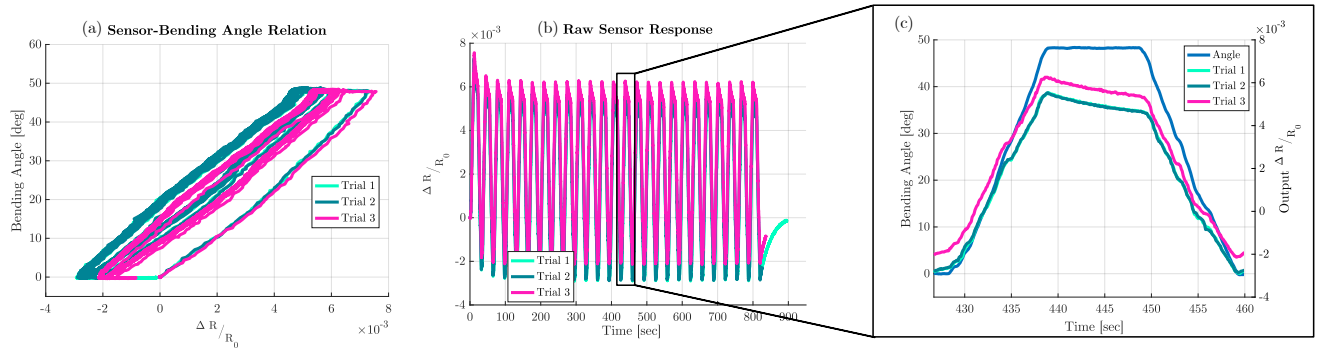

Fig. 7. CPPR cyclic loading experiment. (a): Sensor response to bending angle. (b): Raw sensor output. (c): Enlarged view of the sensor's response to CPPR bending.

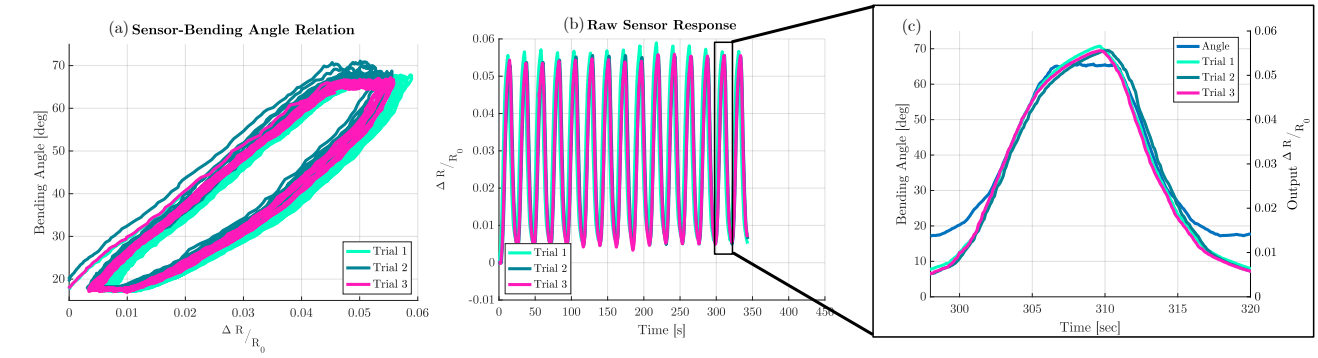

Fig. 8. NWT cyclic loading experiment. (a): Sensor response to bending angle. (b): Raw sensor output. (c): Enlarged view of the sensor's response to NWT bending.

The use of liquid metal ink can pose a challenge in that it must be fully encapsulated to prevent oxidation, leakage, and mechanical degradation over time. Although TPU encapsulation proved to be sufficient for the sensors to withstand the bending tests reported in this letter, it is possible that prolonged use could compromise sensor integrity. Future work should therefore include fatigue testing to study sensor durability and, if necessary, the development of enhanced encapsulation strategies to improve mechanical robustness.

An important limitation of the sensors described in this manuscript is their ability to measure only the total strain of a continuum robotic arm as a whole. These sensors perform well for robots bending in a constant curvature arc but are not suitable for robots that deform into more complex shapes. To address this limitation, future work will focus on extending the current approach to enable local strain measurements. This could be achieved, for instance, by fabricating an array of miniaturized strain gauges distributed along the robot's body. Although this solution is not explored in the present manuscript, we believe that our sensor fabrication method holds promise for producing such miniaturized sensors, thanks to the ability to print traces as small as $0.3\,\mathrm{mm}$.

V. Conclusion

This paper presented the design, fabrication, and experimental characterization of stretchable strain sensors for the shape sensing of continuum robots. Among the different sensor materials evaluated in the study, gallium-indium eutectic emerged as the most suitable for the application at hand, enabling the creation of sensors with minimal drift and high linearity. Experimental findings demonstrate the viability of the proposed sensors for shape sensing at both centimeter and millimeter scales.

Future directions for this work include sensor calibration, focusing on modeling the observed hysteresis and "break-in" behavior. Additionally, this proof-of-principle study was limited to unidirectional bending. In practical applications, multiple sensors would be required to monitor multiple sections of a continuum robot, enabling local shape sensing under complex bending conditions. Exploring these scenarios represents another key area of focus for our future work.

References

[1] M. Russo, S. M. H. Sadati, X. Dong, A. Mohammad, I. D. Walker, C. Bergeles, K. Xu, and D. A. Axinte, "Continuum robots: An overview," *Advanced Intelligent Systems*, vol. 5, no. 5, p. 2200367, 2023.

[2] P. E. Dupont, N. Simaan, H. Choset, and C. Rucker, "Continuum robots for medical interventions," *Proceedings of the IEEE*, vol. 110, no. 7, pp. 847–870, 2022.

[3] J. Burgner-Kahrs, D. C. Rucker, and H. Choset, "Continuum robots for medical applications: A survey," vol. 31, no. 6, pp. 1261–1280, 2015.

[4] Q. Qi, G. Qin, Z. Yang, G. Chen, J. Xu, Z. Lv, and A. Ji, "Design and motion control of a tendon-driven continuum robot for aerospace applications," *Proceedings of the Institution of Mechanical Engineers, Part G: Journal of Aerospace Engineering*, p. 09544100241263004, 2024.

IEEE Robotics and Automation Letters (RA-L) paper, presented at ICRA 2026, Vienna, Austria. Cite as RA-L paper.

[5] M. Russo, L. Raimondi, X. Dong, D. Axinte, and J. Kell, "Task-oriented optimal dimensional synthesis of robotic manipulators with limited mobility," *Robotics and Computer-Integrated Manufacturing*, vol. 69, p. 102096, 2021.

[6] M. M. Coad, L. H. Blumenschein, S. Cutler, J. A. R. Zepeda, N. D. Naclerio, H. El-Hussieny, U. Mehmood, J.-H. Ryu, E. W. Hawkes, and A. M. Okamura, "Vine robots," *IEEE Robotics & Automation Magazine*, vol. 27, no. 3, pp. 120–132, 2019.

[7] C. Shi, X. Luo, P. Qi, T. Li, S. Song, Z. Najdovski, T. Fukuda, and H. Ren, "Shape sensing techniques for continuum robots in minimally invasive surgery: A survey," *IEEE Transactions on Biomedical Engineering*, vol. 64, no. 8, pp. 1665–1678, 2016.

[8] C. Shentu, E. Li, C. Chen, P. T. Dewi, D. B. Lindell, and J. Burgner-Kahrs, "Moss: Monocular shape sensing for continuum robots," *IEEE Robotics and Automation Letters*, vol. 9, no. 2, pp. 1524–1531, 2024.

[9] J. M. Ferguson, D. C. Rucker, and R. J. Webster, "Unified shape and external load state estimation for continuum robots," *IEEE Transactions on Robotics*, vol. 40, pp. 1813–1827, 2024.

[10] C. Gao, H. Phalen, S. Sefati, J. Ma, R. H. Taylor, M. Unberath, and M. Armand, "Fluoroscopic navigation for a surgical robotic system including a continuum manipulator," *IEEE Transactions on Biomedical Engineering*, vol. 69, no. 1, pp. 453–464, 2022.

[11] C. Zhang, C. Hu, Z. He, Z. Fu, L. Xu, G. Ding, P. Wang, H. Zhang, and X. Ye, "Shape estimation of the anterior part of a flexible ureteroscope for intraoperative navigation," *International Journal of Computer Assisted Radiology and Surgery*, vol. 17, no. 10, pp. 1787–1799, 2022.

[12] Y.-J. Zhao, C. Wen, Y.-D. Zhang, and H. Zhang, "Needle tip pose estimation for ultrasound-guided steerable flexible needle with a complicated trajectory in soft tissue," *IEEE Robotics and Automation Letters*, vol. 7, no. 4, pp. 11 705–11 712, 2022.

[13] H. Su, G. Li, D. C. Rucker, R. J. Webster III, and G. S. Fischer, "A concentric tube continuum robot with piezoelectric actuation for mri-guided closed-loop targeting," *Annals of biomedical engineering*, vol. 44, pp. 2863–2873, 2016.

[14] S. Lilge, T. D. Barfoot, and J. Burgner-Kahrs, "Continuum robot state estimation using gaussian process regression on se (3)," *The International Journal of Robotics Research*, vol. 41, no. 13-14, pp. 1099–1120, 2022.

[15] S. Song, H. Ge, J. Wang, and M. Q.-H. Meng, "Real-time multi-object magnetic tracking for multi-arm continuum robots," *IEEE Transactions on Instrumentation and Measurement*, vol. 70, pp. 1–9, 2021.

[16] A. W. Mahoney, T. L. Bruns, P. J. Swaney, and R. J. Webster, "On the inseparable nature of sensor selection, sensor placement, and state estimation for continuum robots or "where to put your sensors and how to use them"," in *2016 IEEE International Conference on Robotics and Automation (ICRA)*, 2016, pp. 4472–4478.

[17] Y. Chitalia, N. J. Deaton, S. Jeong, N. Rahman, and J. P. Desai, "Towards fbg-based shape sensing for micro-scale and meso-scale continuum robots with large deflection," *IEEE Robotics and Automation Letters*, vol. 5, no. 2, pp. 1712–1719, 2020.

[18] S. Sefati, R. J. Murphy, F. Alambeigi, M. Pozin, I. Iordachita, R. H. Taylor, and M. Armand, "Fbg-based control of a continuum manipulator interacting with obstacles," in *2018 IEEE/RSJ International Conference on Intelligent Robots and Systems (IROS)*, 2018, pp. 6477–6483.

[19] R. Xu, A. Yurkewich, and R. V. Patel, "Curvature, torsion, and force sensing in continuum robots using helically wrapped fbg sensors," *IEEE Robotics and Automation Letters*, vol. 1, no. 2, pp. 1052–1059, 2016.

[20] S. C. Ryu and P. E. Dupont, "Fbg-based shape sensing tubes for continuum robots," in *2014 IEEE International Conference on Robotics and Automation (ICRA)*, 2014, pp. 3531–3537.

[21] Q. Zhao, J. Lai, K. Huang, X. Hu, and H. K. Chu, "Shape estimation and control of a soft continuum robot under external payloads," *IEEE/ASME Transactions on Mechatronics*, vol. 27, no. 5, pp. 2511–2522, 2022.

[22] S. Zhao, D. Liu, and F. Yan, "Wearable resistive-type stretchable strain sensors: Materials and applications," *Advanced Materials*, vol. 37, no. 5, p. 2413929, 2025.

[23] K. Oliver-Butler, J. A. Childs, A. Daniel, and D. C. Rucker, "Concentric push–pull robots: Planar modeling and design," *IEEE Transactions on Robotics*, vol. 38, no. 2, pp. 1186–1200, 2021.

[24] S. Ma, J. Tang, T. Yan, and Z. Pan, "Performance of flexible strain sensors with different transition mechanisms: A review," *IEEE Sensors Journal*, vol. 22, no. 8, pp. 7475–7498, 2022.

[25] H. Liu, H. Zhang, W. Han, H. Lin, R. Li, J. Zhu, and W. Huang, "3d printed flexible strain sensors: from printing to devices and signals," *Advanced Materials*, vol. 33, no. 8, p. 2004782, 2021.

[26] H. Souri, H. Banerjee, A. Jusufi, N. Radacsi, A. A. Stokes, I. Park, M. Sitti, and M. Amjadi, "Wearable and stretchable strain sensors: materials, sensing mechanisms, and applications," *Advanced Intelligent Systems*, vol. 2, no. 8, p. 2000039, 2020.

[27] E. M. Abbara, M. Alhendi, R. Al-haidari, N. Gee, M. D. Poliks, E. Boggs, T. Yewteck, D. Trivedi, Z. j. Farrell, and C. E. Tabor, "Electromechanical and thermal characterization of printed liquid metal ink on stretchable substrate for soft robotics multi-sensing applications," in *2023 IEEE 73rd Electronic Components and Technology Conference (ECTC)*, 2023, pp. 426–431.

[28] A. Koivikko, E. Sadeghian Raei, M. Mosallaei, M. Mäntysalo, and V. Sariola, "Screen-printed curvature sensors for soft robots," *IEEE Sensors Journal*, vol. 18, no. 1, pp. 223–230, 2018.

[29] J. A. Childs and C. Rucker, "A kinetostatic model for concentric push–pull robots," *IEEE Transactions on Robotics*, vol. 40, pp. 554–572, 2024.

[30] N. E. Pacheco, J. B. Gafford, M. A. Atalla, R. J. Webster, and L. Fichera, "Beyond constant curvature: A new mechanics model for unidirectional notched-tube continuum wrists," vol. 06, no. 1, p. 2140004.

[31] D. F. Fernandes, C. Majidi, and M. Tavakoli, "Digitally printed stretchable electronics: a review," *Journal of Materials Chemistry C*, vol. 7, no. 45, pp. 14 035–14 068, 2019.

[32] R. Zhang, M. Baxendale, and T. Peijs, "Universal resistivity–strain dependence of carbon nanotube/polymer composites," vol. 76, no. 19, p. 195433.

[33] L. Flandin, Y. Bréchet, and J.-Y. Cavaillé, "Electrically conductive polymer nanocomposites as deformation sensors," vol. 61, no. 6, pp. 895–901.

[34] R. Hibbeler, *Mechanics of Materials*. Pearson Education Limited, 2023.

[35] W. Zhang, Q. Liu, and P. Chen, "Flexible strain sensor based on carbon black/silver nanoparticles composite for human motion detection," *Materials*, vol. 11, no. 10, p. 1836, 2018.

[36] P. J. Swaney, P. A. York, H. B. Gilbert, J. Burgner-Kahrs, and R. J. Webster, "Design, fabrication, and testing of a needle-sized wrist for surgical instruments," vol. 11, no. 1, p. 014501.

[37] Y. Chen, J. M. Oliveira, and I. W. Hunter, "Two-axis bend sensor design, kinematics and control for a continuum robotic endoscope," in *2013 IEEE International Conference on Robotics and Automation*, 2013, pp. 704–710.

[38] M. Semenov, S. Borzunov, P. Meleshenko, and N. Sel'Vesyuk, "The preisach model of hysteresis: fundamentals and applications," *Physica Scripta*, vol. 99, no. 6, p. 062008, 2024.